International Research Journal of Engineering and Technology (IRJET) e-ISSN: 2395-0056
Volume: 09 Issue: 11 | Nov 2022 www.irjet.net p-ISSN: 2395-0072

An imaging and measurement system for the Plasma Arc Welding

Sandeep Kumar[1], Amit Kumar[2]

[1]*Asst. Prof., Department of Mechanical Engineering, Swami Vivekanand Subharti University (U.P), India*
[2] *Asst. Prof., Department of Mechanical Engineering, Swami Vivekanand Subharti University (U.P), India*

Abstract - *To better understand the complex welding processes the automatic and flexible geometry measurement of the weld pool surface can help and can also provide feedback to better control this process. An additional source of illumination is used in most of the existing imaging systems to remove the light interference coming from the welding arc. But it is usually costly. This paper introduces a novel low-cost optical-sensor-based monitoring system working under passive mode to monitor the wire + arc additive manufacturing process, particularly for plasma arc welding. Initially, configurations and parameters of the camera are investigated to achieve good visualization of the weld pool. To perform this procedure a new camera calibration method is proposed using the nozzle of a computer numerical control (CNC) machine imaging system, estimating the position of the camera concerning the inspection surface and its orientation in an easy-to-use approach. allows. Verification tests show that the average error of calibration is less than 1 pixel. To measure the width of the bead during the welding process, an image analysis routine is proposed, as a case study. The results analysis shows that the proposed system is effective to measure the dimension of the weld pool.*

Key Words: **Additive manufacturing, camera calibration, edge detection, plasma arc welding, wire + arc additive manufacture**

1. INTRODUCTION

ADDITIVE manufacturing is defined as a process of three-dimensional printing in which parts are built by adding materials layer by layer. Compared to traditional subtractive manufacturing technologies, this technique allows a high reduction in costs by substantially saving material and reducing lead time. It also offers higher flexibility in the design. Wire + arc additive manufacture (WAAM) uses an electric arc as the power source and wire as the feedstock, which is one of the most promising techniques of AM under development. WAAM is suitable for medium-large scale manufacturing and is being widely used in areas such as the aerospace industry, particularly where the need for the manufacture of titanium parts is increasing significantly due to its chemical compatibility with composites. It also offers a cleaner working environment, higher deposition rates, and less risk of contamination when compared with the powder-based system. The dimensions and geometry of the final piece are very much influenced due to fluctuations in parameters and working conditions in the WAAM. Changes in operating parameters, heat dissipation, interlayer temperature, and quality of the back layer are among the main factors requiring significant investigation. To deal with these, the process needs to be monitored and ideally controlled. An optimistic approach is to use visualization techniques to track the weld pool geometry allowing monitoring of the process or potentially implementing a closed-loop control system. Only a few research works have been reported in the field of AM regarding optical sensing and corresponding reliable measurement, but several techniques have been implemented for the automation and enhancement of welding processes.

The harsh conditions like melting and deposition of the metal play a challenging task in taking the high-quality images of the weld pool during the WAAM process. High-intensity light radiation due to the high temperature of the arc interferes with the image acquisition process. This paper proposed to use a high-shutter-speed camera synchronized with a pulsed laser as an additional source of illumination in gas tungsten arc welding. The camera has a filter that is opaque to all radiation except the laser wavelength, as the laser is monochromatic, which helps the system work. This greatly reduces the intensity of the plasma light for the laser light to be seen. One solution is to use an array of low-cost semiconductor laser diodes and a suitable bandpass filter matched to the laser wavelength, in place of higher-cost equipment such as camera heads, laser units, and controllers. use has been proposed. Recently, some improved methods of reconstructing 3-D weld pool geometry assisted by lasers have been developed. In these processes, an additional source of light has been used to measure the size of the weld pool indirectly rather than to reduce arc interference. Using a laser with a dot-matrix structured light pattern, to reflect the light into an image plane, the weld pool surface can be used as a specular mirror. The camera records the plane of the laser dots being reflected, not the weld pool directly. The system attracts less interest for WAAMs operating under an imaging passive mode than for an active mode. In this process the arc light is used to illuminate the scene; however, accurate calibration of the camera position and a precise selection of a narrow-band filter to reduce the arc light is required in this process. To enhance and automate the welding processes or extract different features from the weld pool for gas metal arc welding based on AM, some research works using passive vision have been reported. A method of using a passive vision system for monitoring the wire deviation during the WAAM process is introduced in recent research. In addition,

infrared (IR) cameras have been used to monitor the weld pool; Still, in obtaining high-quality IR images arc interference poses a major problem.

In terms of the properties to measure using a camera, most of these research works focus on the step height between subsequence layers, the width of the bead, and the height (nozzle to top surface distance). Accurate measurement of these properties is critical to having better control of the WAAM process based on the input parameters, such as the arc current, the wire feeding rate, the travel speed, etc. Although identification of the optimal properties to monitor the weld pool is not the scope of this paper, a case study using the proposed imaging system to measure the width of the weld pool is presented.

Plasma arc welding has fewer transfer modes than GMAW processes due to the metal wire not being the electrode, hence it is a more stable process. When compared to other additive layer manufacturing processes it also allows a higher deposition rate and greater effective wall width. Due to these advantages, it is believed that PAW has great potential and will attract more and more interest in the future. Plasma arc welding has a very bright arc compared to GMAW; this will greatly increase the complexity of image processing. When facing this challenge, developing a reliable and tailored weld pool monitoring system is, therefore, a timely and highly demanded process. To our knowledge, very few passive imaging systems have been developed for the plasma arc welding process due to the challenge of lighting conditions and calibration. This paper introduces a flexible optical-sensor-based monitoring system without additional lighting sources to measure the geometry of the weld pool in the plasma arc welding process. When accommodating the measurement of different properties, an easy-to-use calibration routine is developed to convert the measurement on an image plane to the world coordinate system. Such research will be particularly useful for imaging systems based on a single camera that is required to change position regularly to measure different properties or based on multiple cameras at different positions.

2. Imaging System Setup

A CNC machine, a plasma welding power source, and a wire feeder are combined to implement the plasma arc welding process in this experiment.

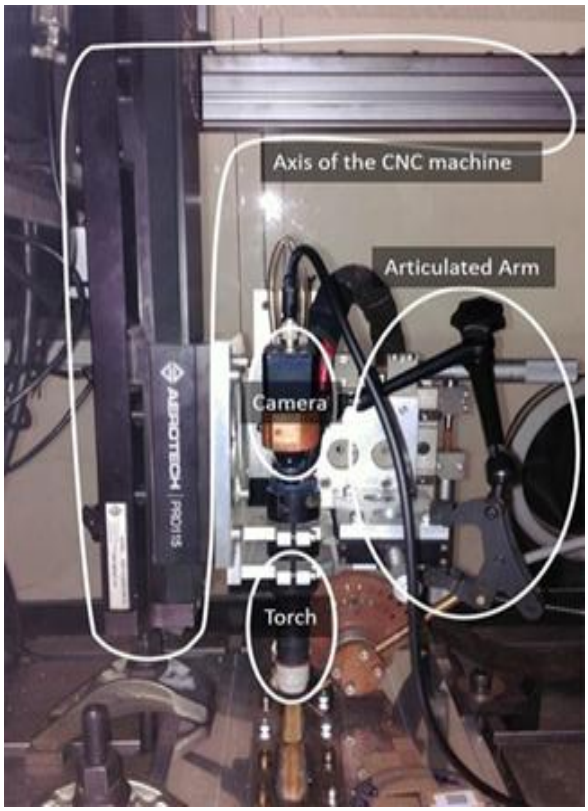

Fig-1. Experimental Setup.

Additionally, the MC500S Weld Vision Camera System, a special welding camera, is used for monitoring the process. A video controller module allows changing gain, intensity, and shutter speed to which the camera is connected. As we can observe from figure 1, the camera is mounted on the moving panel of this computer numerical control (CNC) gantry, with the help of an articulated arm. The relative position between the camera and the torch remains the same during the deposition process because the torch is mounted on the same moving panel of the CNC machine. All the equipment mentioned above is set up inside a chamber. To avoid the oxidation of titanium while the deposition is being processed the chamber is used to create an atmosphere of inert gas, with argon. Because the torch is very close (about 8 mm) to the substrate during the welding process, which the camera will be calibrated toward, LEDs used at the corners light will most likely be blocked by the computer numerical control machine and the torch. Such a setting will introduce shadows in the calibration grid, which will make the image processing more complicated. An additional cable also must be set up in the already crowded CNC machine. While measuring specific properties from the images, the location of the camera plays an important role in determining the quality of the images. To find out the best configuration of the camera, several experiments were conducted with different camera positions, as illustrated in Fig. 2. The wire can be visible with the help of the left setup, but the visual quality of the weld pool is poor due to a large amount of welding arc and the specular surface of the weld pool. In the middle image,

the wire can be observed clearly much similar to the previous one, but the visualization of the weld pool is still very much affected by a large amount of arc light. When we are observing in the right setup, provides the best view of the weld pool with less reflection, but in this setup, wire is not visible. In this experiment mainly focus was on the measurement of the width of the weld pool only, so the right setup was used.

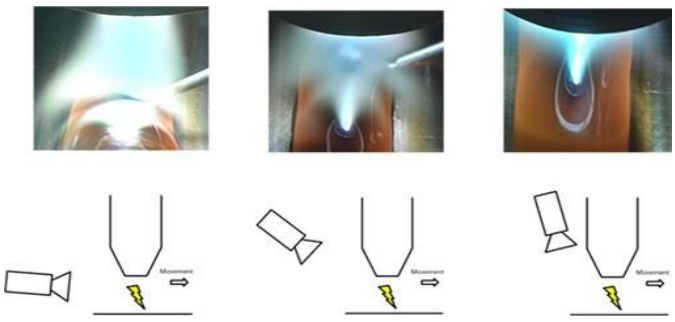

Fig. 2. Captured images with different camera positions.

3. Proposed Calibration and Measurement System

A. Mathematical Background of Camera Calibration

The camera calibration is the process of estimating the intrinsic and distortion parameters of the imaging sensor and lens, and extrinsic parameters concerning the object for measurement. These parameters define how a point in the 3-D world is projected into the image plane, and they are the key to measuring the geometry of an object, correcting lens distortions, or finding the position of the camera. Without considering distortion, the equation

$$\begin{bmatrix} u_i \\ v_i \\ 1 \end{bmatrix} = k[R_{cw} \cdot t_{cw}] \begin{bmatrix} X_c \\ Y_c \\ z_c \\ 1 \end{bmatrix} \quad \text{..... (1)}$$

maps any 3-D point in the world coordinate system to the image plane, where {ui, vi} are the ideal coordinates in the unit of the pixel of the image and $\{X_C, Y_C, Z_C\}$ is a 3-D point in the world coordinate system. The symbol K corresponds to a 3 × 3 matrix containing the intrinsic parameters, and $[R_{CW} \cdot T_{CW}]$ corresponds to a 3 × 4 matrix containing the extrinsic parameters (a rotation matrix and a translation vector), which denotes the transformation from the 3-D world coordinate to the 3-D camera coordinate. Equivalently, the extrinsic parameters define the position of the camera center and the camera's heading in the world coordinate.

In photography, distortion is generally referred to as an optical aberration that deforms and bends the physically straight line and makes them curvy in images. The distortion is caused by the lens. Generally, we can be described distortion by five parameters

{k1 k2 k3 p1 p2} ..... (2)

where p1 and p2 are tangential parameters and k1, k2, and k3 are radial parameters. The correct distortion models can be written as

$$u_r = (1 + k_1 r^2 + k_2 r^4 + k_3 r^6)u_i + 2^p 1^{u_i v} i + p_2(r^2 + 2u_i^2)$$

..... (3)

$$v_r = (1 + k_1 r^2 + k_2 r^4 + k_3 r^6)v_i + 2^p 2^{u_i v} i + p_1(r^2 + 2v_i^2)$$

..... (4)

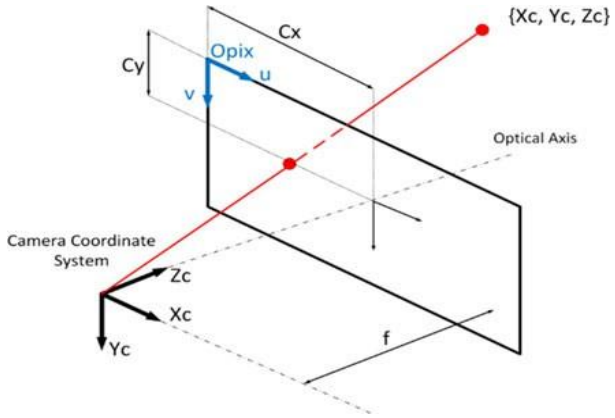

Fig-3. Pinhole camera model with intrinsic parameters.

where $\{u_i, v_i\}$ are the true coordinate in the images and the radial distance of an ideal pixel to the center of the image is r, expressed as

$$r^2 = u_i^2 + v_i^2 \quad \text{..... (5)}$$

Usually, only radial distortion is considered, and tangential parameters are set to zero.

Intrinsic parameters remain constant once the camera and lens is integrated and focused. If the focal length is changed, intrinsic parameters will also change. Intrinsic parameters model the pinhole camera model, which projects any 3-D point from a coordinate system fixed concerning the camera into the image plane. The matrix of the intrinsic parameters can be written as

$$K = \begin{bmatrix} f_x & 0 & C_x \\ 0 & f_y & C_y \\ 0 & 0 & 1 \end{bmatrix} \quad \text{..... (6)}$$

where the focal lengths in the x and y directions are denoted by f_x and f_y respectively. They are in pixels and if assuming square pixels it can be simplified as $f_x = f_y = f$. C_x and C_y correspond to an offset to move the center of the image to the upper left corner. Fig. 3 shows these parameters graphically.

The extrinsic parameters consist of a homogeneous transformation, which includes a rotation and a translation operation. The translation operation consists of vectors from three dimensions, described as

$$t = \{t_x \quad t_y \quad t_z\} \quad \text{..... (7)}$$

For each of the axis, a rotation operation has 3-degrees of freedom corresponding to three angles of rotation, one or each of the axis. In The Euler angles are employed to describe a rotation operation, in this experiment which can be written as

$$R = R_z(\emptyset)\, R_y(\theta)\, R_x(\psi) \quad \text{..... (8)}$$

where $R_y(\theta)$ corresponds to a rotation of θ degree around the y-axis, $R_z(\emptyset)$ corresponds to a rotation of φ degree around the z-axis, and $R_x(\psi)$ corresponds to a rotation of ψ degree around the x-axis. Then, equation (8) can be rewritten as

$$R = \begin{bmatrix} \cos\theta\cos\phi & \sin\psi\sin\theta\cos\phi - \cos\psi\sin\phi & \cos\psi\sin\theta\cos\phi + \sin\psi\sin\phi \\ \cos\theta\sin\phi & \sin\psi\sin\theta\sin\phi + \cos\psi\cos\phi & \cos\psi\sin\theta\sin\phi - \sin\psi\cos\phi \\ \sin\theta & \sin\psi\cos\theta & \cos\psi\cos\theta \end{bmatrix} \quad \text{..... (9)}$$

Note that the extrinsic parameters depend on the location of the camera. Any movement of the camera will require recalculation of these parameters.

B. Calibration Methodology

The proposed calibration method requires taking multiple photographs of the calibration pattern from more than one perspective to improve accuracy. In this paper, a checkerboard, which is a well-accepted calibration pattern in many researches, has been used. If the size of the chessboard square is determined, the 3-D world coordinates of the points on the grid can also be estimated, using the world coordinate system on it. The calibration process consists of solving a system of equations to find the intrinsic, distortion, and extrinsic parameters, which are the ones that relate any 3-D world point with a pixel position on the image plane. Hence, by knowing the 3-D world coordinate of the checkerboard points and knowing the 2-D pixel position corresponding to each of these points, a system of equations can be solved to find all the necessary parameters. Note that theoretically only one pair of 3-D–2-D points would be needed for each parameter, but as aforementioned increasing the number of points the error can be reduced by averaging the results.

Generally, during calibrating on a camera, the procedure is simply moving a calibration pattern in front of a fixed camera. During this process, some problems arose when trying this approach.

1) The calibration pattern must be very small (15 mm × 10.5 mm) because the camera has a narrow field of view. It makes difficult to move the pattern only with small handshaking.

2) There are many elements such as the CNC machine, the torch, or the chamber itself that would limit the movement of the calibration grid, once the camera is fixed.

3) The fact is that all equipment inside a chamber leads to a lack of light. If the grid is moved, a lamp to illuminate it must be moved too, due to which this process became very complicated.

In this paper, the camera will be moved with respect to the calibration pattern, which will remain fixed, to overcome these problems, instead of moving the calibration pattern concerning the camera. Even though such a routine has been generally used in the calibration of many applications, its application is new in plasma arc welding monitoring. Furthermore, to estimate the camera's position, the proposed methodology uses the position of the nozzle concerning the world origin, which can be obtained by using the position of the nozzle displayed by the CNC machine interface. It is noted that the problems listed in the above three main points, sometimes do not apply because internal camera calibration usually does not need to be conducted online.

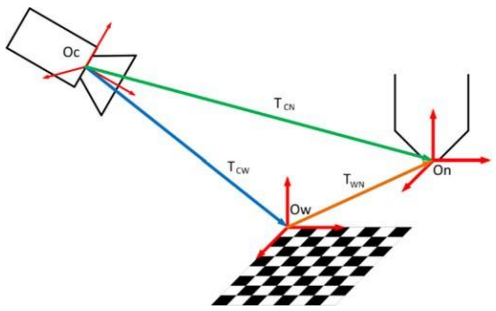

Fig. 4. The coordinate systems representation and transformations involved in measuring the camera pose.

If except for adjusting the lens, it is an offline step that does not depend on the surrounding equipment. The proposed calibration routine can be summarized as follows.

1) To place the calibration grid on the plane where the deposition process will be undertaken.

2) Calculate the position of the world origin in the Computer Numerical Control (CNC) coordinate.

3) Focus the camera considering its location.

4) Move the camera to capture pictures of the calibration grid from different angles of view. While moving the camera, the difference between two consecutive pictures should be noticeable. It is suggested to take pictures when the grid's row lines and column lines are not parallel in the image. A picture taken from exactly the top of the grid, where the lines are parallel, will contain less information.

5) Estimate the intrinsic and distortion coefficients by using the captured pictures in step 4.

6) Fix the camera to the position where the recording of the process will be conducted, take a picture of the calibration pattern and record the position of the CNC machine.

7) Estimate the extrinsic parameters by using the captured picture in step 6.

C. Camera Localization

The location of the camera determines the quality of the images received. The proposed imaging system also allows automatic localization of the camera. The position of the camera for the nozzle will not change, as the camera is mounted with an articulated arm mounted on the moving system. Since the calibration grid can be fixed wherever convenient, the position of the camera should be calculated for a point on the moving elements of the CNC machine. The solution to this system is to use an intermediate coordinate system at the nozzle. This fig. 4 that the external parameters obtained in step 7 of the blue change calibration routine compose these. It acts as a rotation and translation transformation to convert the camera coordinate system to the world coordinate system. Orange Transformation The task of converting the world coordinate system to the nozzle coordinate system is done by the orange transformation. To estimate this can be done by computing the difference between the position of the CNC machine in the world origin and the position of the CNC machine recorded in step 6. Note that this transformation will only involve a translation between the two coordinate systems, but will not involve any rotation.

We know the blue transformation matrix

$$T_{CW} = \{R_{CW} \quad t_{CW}\} \quad \text{..... (10)}$$

and the orange transformation matrix

$$T_{WN} = \{R_{WN} \quad t_{WN}\} \quad \text{..... (11)}$$

the green transformation matrix

$$T_{CN} = \{R_{CN} \quad t_{CN}\} \quad \text{..... (12)}$$

which corresponds to the location of the nozzle with respect to the camera, can be estimated by

$$T_{CN} = T_{CW}.T_{WN} \quad \text{..... (13)}$$

The homogeneous transformation is 4 × 4 matrices composed of a 3 × 3 rotation matrix, a 3 × 1 translation vector, and the scaling factor.

Once the nozzle position in the camera coordinate (green transformation) is estimated, the last step is to invert this transformation to obtain the camera's position with respect to the nozzle coordinate system. Note that the camera coordinates of the system are always defined with the z-axis pointing to the direction in which the camera is recording. To reduce computational time, without inverting the 4 × 4 transformation matrix, the camera rotation matrix and translation vector can be calculated based on the green transformation described by (14) and (15), respectively,

$$R_{NC} = (R_{CN})^T \quad \text{..... (14)}$$

$$t_{NC} = -R_{NC}.t_{CN}. \quad \text{..... (15)}$$

D. Measuring Real Distance

The major problem that occurs during traducing the measure from pixels to real-world units is that there is a loss of information, particularly the depth when taking a picture and projecting the 3-D coordinates of an object into the image plane (2-D). For every pixel in the image, there is an infinite number of possible locations in the 3-D space. To measure distances and angles on the images, recovering this lost information is essential.

To address these types of problems stereo vision is a well-known technique. It uses the principle of having the same two points in both images, and therefore finding the intersection of the two-pixel rays the 3-D depth information can be recovered. In the present case, this technique is not possible because only a single camera is used. Hence, some extra geometrical information is needed to find the 3-D coordinate from a 2-D pixel. The plane equation in which we know the desired pixel will be contained, the extra information that can be used. For instance, the plane that contains the two edges of the bead is a plain in which the welding is taking place during the measuring of the bead width.

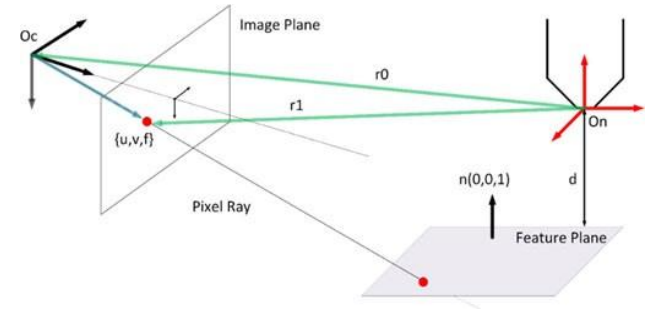

Fig-5. Pixel ray projection into the feature plane to recover 3-D information

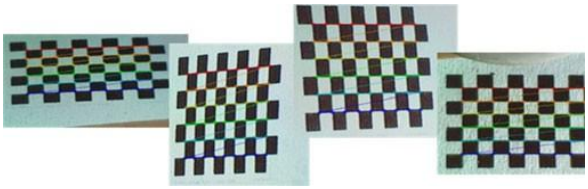

Fig-6. Different pictures from different camera positions of the calibration pattern.

Fig. 5 shows this concept in detail. To project the pixel into the feature plane and recover the 3-D coordinate, the intersection between the pixel ray line and the plane must be found. By using the intrinsic and extrinsic parameters obtained previously with the camera calibration the equation of the pixel projection line can be solved.

The vector equation of a line can be expressed as

$$\vec{r} = \vec{r_0} + \lambda.\vec{m} \quad \text{..... (16)}$$

where $\vec{r_0}$ is a point on the line, and $\vec{m}$ is the line direction. This means $\vec{r}$ would contain any point on the line by varying the distance $\lambda \in (-\infty, +\infty)$ from $\vec{r_0}$ to this point. To find the vector equation of the pixel ray line in nozzle coordinates, $\vec{r_0}_N$ can be calculated as the camera position, found in the previous section expressed as

$$\vec{r_0}_N = t_{NC} = -R_{NC} \cdot t_{CN} \quad \text{..... (17)}$$

To calculate the direction vector $\vec{m}$, the point $\vec{r_1}$ shown in Fig. 6 can be used. Note that this point in the camera coordinate system corresponds to

$$\vec{r_1}_C = \begin{bmatrix} u \\ v \\ f \end{bmatrix} \quad \text{..... (18)}$$

To transform $\vec{r_1}_C$ from the camera coordinate system to the nozzle coordinate system, the rotation matrix and translation vector is used. The transform can be written as

$$\vec{r_1}_N = R_{NC} \begin{bmatrix} u \\ v \\ f \end{bmatrix} + t_{NC} \quad \text{..... (19)}$$

Hence, the direction vector can be calculated by

$$\vec{m} = \vec{r_1}_N - \vec{r_0}_N = \left(R_{NC} \begin{bmatrix} u \\ v \\ f \end{bmatrix} + t_{NC} \right) - t_{NC} = R_{NC} \begin{bmatrix} u \\ v \\ f \end{bmatrix} \quad \text{..... (20)}$$

Next, once the pixel ray line equation, that defines all the possible 3-D positions of the 2-D pixel, is determined, the intersection with the feature plane is used to recover the exact location among all the infinite possibilities. Having a general normalized plane

$$\vec{n} \cdot \vec{r} = d \quad \text{..... (21)}$$

where $\vec{n}$ is a unit vector normal to the plane and d is the minimum distance from the plane to the origin. Substituting

(16) into (21), the line-plane intersection can be found; the value of λ can be calculated by

$$\lambda = \frac{d - \overrightarrow{r_{0N}} \cdot \vec{n}}{\vec{m} \cdot \vec{n}} \quad \text{..... (22)}$$

4. Results and Discussions

A. Intrinsic and Distortion Parameters

This section corresponds to steps 4 and 5 of the camera calibration methodology explained in Section III-B. to estimate the intrinsic and distortion coefficients, there are a total of 12 positions of the camera have been tested. The resolution of the image is 800 × 600 pixels. Four examples are shown in Fig. 6 that illustrate the detect feature points on the calibration checkerboard to perform the calibration. It is to be noted that the world origin would correspond to the first red point from the top left. Then, the axis will be defined depending on how the successive points are defined in the 3-D space. Because the calibration parameters were calculated by averaging the results from different calibration images, more calibration images usually produce more accurate results. The Visual Studio C++ 2015 and OpenCV library implemented all calibration steps and image processing algorithms.

Assuming square pixels, the detected intrinsic parameters (unit: pixel) are:

$$K = \begin{bmatrix} 8077 \cdot 52 & 0 & 399 \cdot 3 \\ 0 & 8077 \cdot 52 & 299 \cdot 3 \\ 0 & 0 & 1 \end{bmatrix} \quad \text{..... (23)}$$

Based on the matrix shown above we can conclude that f_x = f_y = 8077.52 pixels and the upper left corner with respect to the center of the image is C_x = 399.3 pixels and C_y = 299.3 pixels.

The detected camera distortion parameters are

$$k_1 = 2.93$$
$$k_2 = 1755.7$$
$$k_3 = 5.30 \quad \text{..... (24)}$$

To the raw images we can apply (3) and (4) based on the identified parameters shown in (24) to reduce distortion, which means that the reliability of the measurements can be improved in the next steps. The right picture of Figure 7 shows a difference image between a raw image and the corresponding undistorted image in binary form. One can notice a clear variation at the boundary of the weld pool, which will affect the following measurements.

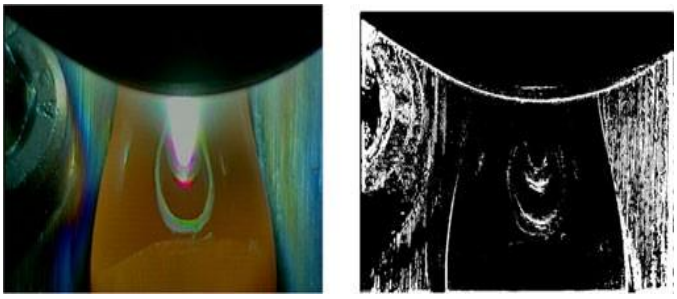

Fig. 7. (Left): A raw image. (Right): The difference between the raw and the undistorted image.

B. Extrinsic Parameters

The position of the camera was fixed on the working place after the intrinsic parameters and distortion parameters are calculated, and one picture of the grid was taken to calculate the extrinsic parameters, as stated in steps 6 and 7 in Section III-B.

To find the orange transformation in Fig. 4. Fig. 7 shows a picture captured from the top position, the position of the nozzle of the CNC machine has been used where the coordinates of the nozzle (unit: mm) are

$$t_{CNC_1} = \{198 \cdot 42 \quad 266 \cdot 61 \quad 244 \cdot 42\} \quad \text{..... (25)}$$

Knowing that the position of the CNC in the world coordinate (in mm) can be converted to

$$t_{CNC_2} = \{180 \cdot 25 \quad 257 \cdot 62 \quad 247 \cdot 29\} \quad \text{..... (26)}$$

the translation vector from the world coordinate system to the nozzle coordinate system (the orange transformation) (in mm) can be calculated by

$$t_{WN} = t_{CNC_1} - t_{CNC_2} = \{18 \cdot 17 \quad 8 \cdot 99 \quad -2.87\} \quad \text{..... (27)}$$

The extrinsic parameters, composed of the rotation and translation from the camera coordinate to the world coordinate (the blue transformation in Fig. 4), are shown in (28) and (29), respectively

$$R_{CW} = \begin{bmatrix} 0 \cdot 9985 & 0.0131 & -0.0442 \\ 0.0016 & 0 \cdot 9446 & 0 \cdot 3265 \\ 0.0442 & -0.3263 & 0.9437 \end{bmatrix} \quad \text{..... (28)}$$

$$t_{CW} = \{-6.42mm \quad -2.70mm \quad -219.68mm\}$$

…….. (29)

Since the nozzle does not rotate concerning the world coordinate system, finally, the camera rotation and translation, concerning the nozzle coordinate system, can be found in (30) and (31), respectively

$$R_{NC} = \begin{bmatrix} 0 \cdot 9985 & 0.0016 & 0.0442 \\ 0.0131 & 0 \cdot 9446 & 0 \cdot 3263 \\ -0.0442 & -0.3265 & 0.9437 \end{bmatrix}$$

…….. (30)

$$t_{NC} = \{-21 \cdot 95mm \quad -65 \cdot 47mm \quad -203.86mm\}$$

…….. (31)

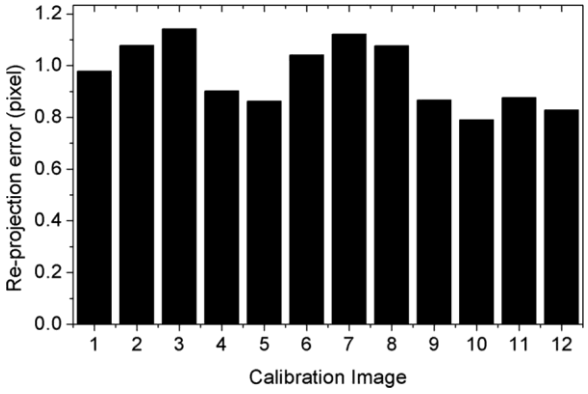

Fig- 8. Reprojection error for each image used in calibration.

The rotation matrix in (30) can also be written as Euler angles, as shown in (32) and (33)

$$\Psi_1 = 19.10^\circ$$
$$\theta_1 = 2.53^\circ$$
$$\emptyset_1 = 0.77^\circ \quad \text{…….. (32)}$$

$$\Psi_2 = -160.87^\circ$$
$$\theta_2 = 177.42^\circ$$
$$\emptyset_2 = -179.20^\circ \quad \text{…….. (33)}$$

The reprojection errors of the calibration process are used to evaluate the accuracy of the calibration. It consists of projecting the 3-D calibration grid points using the estimated calibration parameters and then measuring the mean square error between the projected points and the original points in the image. The12 tests with different positions of the camera have been conducted to estimate the extrinsic parameters. Fig. 8 shows the plot of the reprojection error for every calibration image. In a relatively small range Variation of error has been observed. The average error is 0.964 ± 0.124 pixels. Note the camera positions for the 12 cases are different, which indicates that the extrinsic parameters are different and the scales between the world coordinate and the image coordinate are different. The error in mm would only be valid for a particular case; consequently, it is believed that providing the reprojection error in pixels is more general because it is independent of the scale/distance of the object that is being recorded.

C. Width Tracking

The proposed imaging and calibration system aims to accommodate the measurement of different properties of the weld pool. This section presents a case study to measure the width of the bead to demonstrate this system.

The following two assumptions are made to obtain good results using this procedure.

1) The edge of the welding bead can be found in the images.
2) The desired boundary movement from one frame to another is smooth. This assumption is valid for most cases because the change in width of the welding bead will hardly be abrupt.

The steps to measure the bead width can be described as follows:

1) The distortion parameters are applied as shown in (17) to correct the distortion.
2) Initialize edge points and apply a window: To know where to start tracking the edges of the bead, two edge points are initialized. These points are initialized manually by clicking on the image. The x and y coordinates of the first point as well as the y-coordinate of the second point determines by the first click. The second click determines the x coordinate of the second point. Based on these points, two windows are applied, one for each of the edges, to reduce the region of interest allowing to reduce the number of calculations to process the image and find the edges.
3) Image enhancement: To reduce noise, increase the chance to find the edge, and improve the reliability of measurement, the mean shift filter is applied. The mean shift of the filter is an iterative filter, which produces a color segmentation of the image by processing a certain amount of neighbor pixels with a certain range in the color acceptance to make one particular color region grow progressively.

4) Edge detection: To find reliable edges in an image, the Canny edge detector is used.
5) Thresholding: In this paper, Otsu's thresholding method is employed to remove weak edges and preserve the strong ones.
6) Line extraction: The Hough Transform technique is employed to find lines in a binary image.
7) Line selection: After obtaining a range of possible lines from the Hough Transform, a decision has to be made to select which of the extracted lines corresponds to the boundary of the bead. Because the presence of noise in the image introduces false edges, this step is very essential, which must be filtered before the landmark detection. To address this, several assumptions are made, which are as follows:

    a) only the most reliable ones given by the Hough Transform will be analysed;
    b) the most reliable line will always be the one with the middle point closer to the previous bead corner if this distance is inside a certain threshold; and
    c) If the lines obtained are outside the threshold, the most reliable line will tend to be the one inside the weld pool & that is at the right side for the left edge, and at the left side for the right edge.

8) Landmark detection: The middle point on the selected lines will be used as a landmark to calculate the width.
9) Calculate the width in the unit of "mm" by applying the extrinsic parameters shown in (23) and (24) identified from the calibration procedure.

Fig. 9 illustrates the routine procedure to measure the bead width and the intermediate images corresponding to each step.

Fig. 10 plots the results of bead width measurement for the 40 consecutive frames from two tests using the proposed calibration system and image analysis method, plotted by the solid curves. Fig. 11 shows a snapshot of the welding bead width measurement.

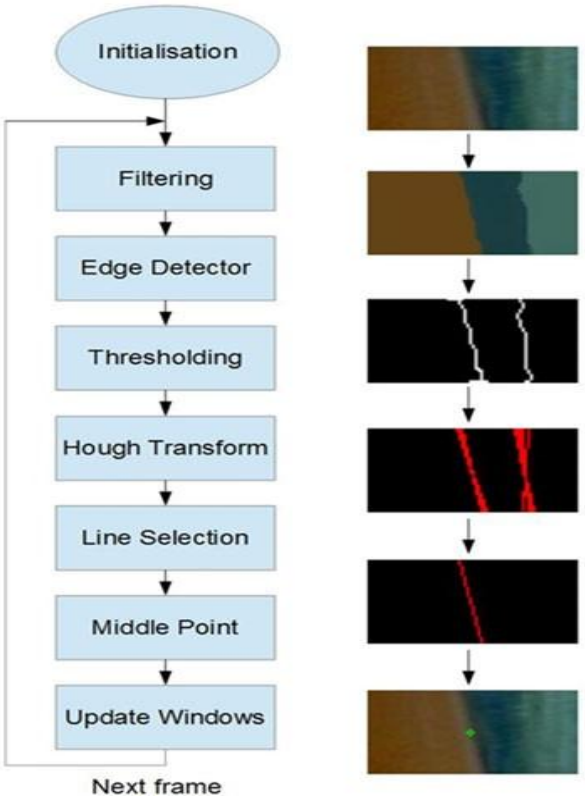

Fig-9. Illustration of the developed width tracking method.

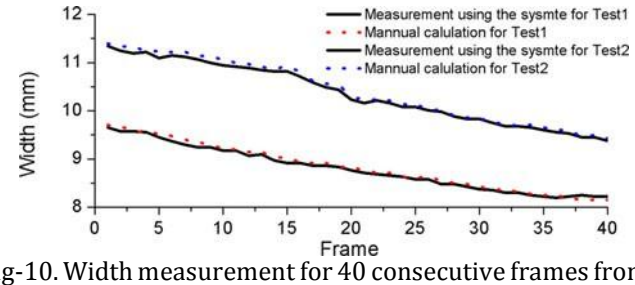

Fig-10. Width measurement for 40 consecutive frames from two tests

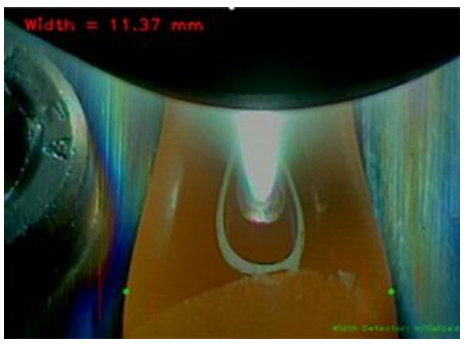

Fig-11. Width measurements for test 1 at frame 1.

To evaluate the accuracy of measurement, the width of the bead was manually measured based on the sampled images and the results are plotted by the dotted curves in Fig. 10. A very good approximation of the ground truth indicates by the visual inspection. The average errors for Tests 1 and 2 are 0.052 ± 0.030 mm and 0.062 ± 0.034 mm, respectively, or 1.48 ± 1.82 and 2.40 ± 1.35 pixels, respectively.

Although this case study focuses on one parameter only, the proposed imaging system can measure multiple parameters at the same time. For example, if the setup shown in Fig. 2(b) is used, both the width of the bead and the position of the wire (e.g., the angle of the wire) can be measured. This case study only demonstrates how to use the said system to measure a parameter. To measure other parameters such a methodology can be easily extended, while the difference would be the feature detection using image processing methods.

5. CONCLUSIONS

The main goal of this research was to investigate how to sense a PAW process through a low-cost computer vision technique in an easy-to-use approach. To achieve this goal, this paper proposed a passive imaging system, which includes a data acquisition setup, a novel calibration routine, feature extraction, and measurement. This system allows the user to track the weld pool geometry online during the welding processing, which can be feedbacked to the controller of experimental parameters to better control this process. The verification tests showed that the average error of calibration is less than 1 pixel. A case study to track the bead width was presented in this paper to demonstrate how the proposed system measures the geometry of the weld pool. A novel routine of feature extraction using an image processing technique was proposed. The results showed that the proposed system can effectively track the dynamics of the bead width.

The main novelty of the research was the calibration methodology, specifically for PAW, which allows transforming measurements from pixel to the real-word unit automatically through an easy-to-use routine and accurately through compensating camera distortion. The proposed calibration moves the camera concerning the calibration pattern on the deposition position instead of moving the calibration pattern due to the space limitation in the CNC machine. Because the position of the camera concerning the nozzle was always the same, the position of the nozzle and the estimated parameters were then used to localize the camera position. The standard calibration process was tailored to better fit the monitoring of the Plasma Arc Welding (PAW) process through such unique changes.

The proposed system features the following key advantages:

1) The camera distortion was considered to improve the measurement accuracy.
2) Having the whole camera model allows the fast and accurate calculation of the camera position in 3-D. This can be especially useful to set up the experimental condition and to perform further experiments by changing the camera positions to improve the image quality or to measure other features of the process.
3) No laser illumination was required, and the whole imaging system was relatively less experience.

The proposed calibration process assumes that the camera has square pixels ($f_x = f_y$) which fits most cameras. If the pixels were not exactly square, the process to estimate intrinsic parameters will not be affected & two independent parameters f_x and f_y will be estimated. However, the current equations (18)-(20) will be affected and need to be extended, which will be one of the future works.

This system is ready to accommodate the measurement of different features either by changing the camera or camera position. Futures works will focus on the following:

1) Identifying the optimal camera position to measure multiple important parameters of the weld pool;
2) 3-Dimensional surface reconstruction of the whole weld pool; and
3) The influence of different control parameters on the geometry of the weld pool.

REFERENCES

[1] L. O. Vilarinho, B. Lucas, and M. Houghton, "Dedicated near-infrared vision system for monitoring welding processes," in Proc. 20th Int. Congr. Mech. Eng., Gramado, Brazil, 2009, pp. 7–13.

[2] H. Song and Y. Zhang, "Measurement and analysis of three-dimensional specular gas tungsten arc weld pool surface," Weld. J., vol. 87, pp. 85–95, 2008.

[3] Z. Wang, "An imaging and measurement system for robust reconstruction of weld pool during arc welding," IEEE Trans. Ind. Electron., vol. 62, no. 8, pp. 5109–5118, Aug. 2015.

[4] J. Zeshi, L. Haichao, J. Guoquing, and G. Hongming, "Dynamic non-linear modeling of 3D weld pool surface in GTAW," Robot. Comput.-Integr. Manuf., vol. 39, pp. 1–8, 2016.

[5] W. Lucas, D. Bertasco, G. Melton, J. Smith, and C. Balfour, "Real-time vision-based control of weld pool size," Weld. Int., vol. 26, no. 4, pp. 243– 250, 2012.

[6] C. Wu, J. Gao, X. Liu, and Y. Zhao, "Vision-based measurement of weld pool constant-current gas tungsten arc welding," Proc. Inst. Mech. Eng., J. Eng. Manuf., vol. 217, pp. 879–882, 2003.

[7] J. Liu, Z. Fan, S. I. Olsen, K. H. Christensen, and J. K. Kristensen, "A real-time passive vision system for robotic arc welding," in Proc. IEEE Int. Conf. Autom. Sci. Eng., 2015, pp. 389–394.

[8] X. Z. Chen, Y. M. Huang, and S. B. Chen, "Model analysis and experimental technique on computing accuracy of seam spatial position information based on stereo vision for welding robot," Ind. Robot, Int. J., vol. 39, no. 4, pp. 349–356, 2012

[9] J. Xiong, G. Zhang, Z. Qiu, and Y. Li, "Vision sensing and bead width control of single-bead multi-layer part: Material and energy saving in GMAW-based rapid manufacturing," J. Cleaner Prod., vol. 41, pp. 82–88, 2012.

[10] J. Xiong and G. Zhang, "Adaptive control of deposited height in GMAWbased layer additive manufacturing," J. Mater. Process. Technol., vol. 214, pp. 962–968, 2013.

[11] J. Xiong and G. Zhang, "Online measurement of bead geometry in GMAW-based additive manufacturing using passive vision," Meas. Sci. Technol., vol. 24, no. 11, 2013, Art. no. 115103.

[12] S. W. Williams, F. Martina, A. C. Addison, J. Ding, G. Pardal, and P. Colegrove, "Wire + arc additive manufacturing," Mater. Sci. Technol., vol. 32, no. 7, pp. 641–647, 2016.

[13] R. Kovacevic, Y. Zhang, and L. Li, "Monitoring of weld joint penetration based on weld pool geometrical appearance," Weld. J., vol. 38, pp. 317– 329, 1996.

[14] Q. Zhan, Y. Liang, J. Ding, and S. Williams, "A wire deflection detection method based on image processing in wire + arc additive manufacturing," Int. J. Adv. Manuf. Technol., vol. 89, pp. 755–763, 2017.

[15] P. Ghanty et al., "Artificial neural network approach for estimating weld bead width and depth of penetration from infrared thermal image of weld pool," Sci. Technol. Weld. Joining, vol. 13, no. 4, pp. 395–401, 2016.

[16] Z. Chen and X. Gao, "Detection of weld pool width using infrared imaging during high-power fiber laser welding of type 304 austenitic stainless steel," Int. J. Adv. Manuf. Technol., vol. 74, no. 9, pp. 1247–1254, 2014.

[17] F. Bonnacorso, L. Cantelli, and G. Muscato, "An arc welding robot control for a shaped metal deposition plant: Modular software interface and sensors," IEEE Trans. Ind. Electron., vol. 58, no. 8, pp. 3126–3132, Aug. 2011.

[18] J. Xiong, Z. Yin, and W. Zhang, "Closed-loop control of variable layer width for thin-walled parts in wire and arc additive manufacturing," J. Mater. Process. Technol., vol. 233, pp. 100–106, 2016.

[19] F. Martina, J. Mehnen, S. Williams, P. Colegrove, and F. Wang, "Investigation of the benefits of plasma deposition for the additive layer manufacture of Ti–6Al–4V," J. Mater. Process. Technol., vol. 212, pp. 1377–1386, 2012

BIOGRAPHIES

Sandeep Kumar (Asst. Prof.), Department of Mechanical Engineering, Subharti University Meerut, M.Tech (Prod.), India.

Amit Kumar (Asst. Prof.), Department of Mechanical Engineering, Subharti University Meerut, M.Tech (Automobile Engg.) NIT Warangal A.P., India